Synthesis, ^{77}Se and ^{119}Sn NMR Study, and X-ray Crystal Structure of the $Sn_4Se_{10}^{4-}$ Anion and Raman Spectra of $SnSe_4^{4-}$ and $Sn_4Se_{10}^{4-}$

Janette Campbell, David P. DiCiommo, Hélène P. A. Mercier, Ayaaz M. Pirani, Gary J. Schrobilgen,* and Marc Willuhn

Department of Chemistry, McMaster University, Hamilton, Ontario L8S 4M1, Canada

Received June 8, 1995[⊗]

The novel selenostannate(IV) anion, $Sn_4Se_{10}^{4-}$, has been obtained by extracting the ternary alloy $KSn_{0.67}Se_{1.93}$ in ethylenediamine (en) and liquid NH_3 in the presence of 2,2,2-crypt (4,7,13,16,21,24-hexaoxa-1,10-diazabicyclo-[8.8.8]hexacosane) and characterized in solution by ^{77}Se and ^{119}Sn NMR spectroscopy and in the solid state by X-ray crystallography and Raman spectroscopy. The scalar couplings, $^1J(^{119}Sn-^{77}Se)$ and $^2J(^{119}Sn-^{117}Sn)$, have been determined and compared with those of related systems. The salt, $(2,2,2\text{-crypt-}K^+)_4Sn_4Se_{10}^{4-}$, crystallizes in the triclinic system, space group $P\bar{1}$, with $Z = 2$ and $a = 14.769(2)$ Å, $b = 15.580(1)$ Å, $c = 26.275(4)$ Å, $\alpha = 79.19(1)°$, $\beta = 85.65(1)°$, and $\gamma = 85.870(8)°$ at 24 °C. The solid state and solution anion geometry is of the adamantanoid type where the Sn^{IV} atoms occupy the bridgehead positions and the Se atoms occupy the bridging and terminal sites. The terminal [average, 2.425(2) Å] and bridging [average, 2.548(2) Å] Sn−Se bond distances were found to correlate with their respective $^1J(^{119}Sn-^{77}Se)$ coupling constants. The Raman spectrum of the $Sn_4Se_{10}^{4-}$ anion has been assigned and compared to those of related adamantanoid systems and $SnSe_4^{4-}$.

Introduction

A structural unit frequently encountered in the chemistry of heavy main-group metal chalcogenide anions is the adamantanoid M_4Ch_{10} or $M_4Ch_6R_4$ cage [R = Ch, halide (X), organic or organometallic fragments]. The structures contain M_4Ch_6 cores with the Ch, X, or R substituents in the terminal positions. To date, adamantanoid compounds containing Group 12 [$Hg_4(\mu\text{-ChR})_6X_4^{2-}$,[1] $M_4(\mu\text{-SePh})_6(SePh)_4^{2-}$,[2] $Hg_4(\mu\text{-SR})_{6-m}(\mu\text{-X})_mX_4^{2-}$ [3] (M = Zn, Cd; Ch = S, Se, Te; R = Et, *n*-Pr, *i*-Pr, *n*-Bu; X = Cl, Br; $m = 0-2$)], Group 13 [$Ga_4S_{10}^{4-}$, $In_4Ch_{10}^{4-}$ (Ch = S, Se)[4]], and Group 14 [$Si_4S_{10}^{4-}$,[5] $Ge_4Ch_{10}^{4-}$ (Ch = S,[5-7] Se,[8,9] Te[10]), $(CH_3)_4Sn_4Ch_6$ (Ch = S,[11] Se[12]), $\{Cp(CO)_2Fe\}_4Sn_4Se_6$,[13] $\{Cp(CO)_3Mo\}_4Sn_4Te_6$[14]] metals have been synthesized and characterized primarily by X-ray crystallography and, to a lesser extent, by vibrational spectroscopy. Dean and co-workers[1-3] have used ^{77}Se, ^{125}Te, ^{111}Cd, ^{113}Cd, and ^{199}Hg NMR spectroscopy to characterize Group 12 adamantanoid cages in solution. Multi-NMR studies of adamantanoid M_4Ch_{10} cages have the potential to provide corroborating structural information in solution and in the form of chemical shifts and M−Ch spin−spin coupling constants which may correlate with structural parameters and vibrational frequencies observed in the solid state.

Our recent investigations on classically-bonded tin(IV) chalcogenide systems obtained by extracting ternary K/Sn/Ch (Ch = Se, Te) alloys in ethylenediamine (en) and liquid NH_3 in the presence of nonstoichiometric amounts of 2,2,2-crypt with respect to K^+, where K^+:2,2,2-crypt = 1.00:0.42 (Se) and 1.00:0.00 (Te), have led to the synthesis and characterization of the ditin(IV) $Sn_2Ch_6^{4-}$ and $Sn_2Ch_7^{4-}$ anions and the tetratin(IV) adamantanoid $Sn_4Se_{10}^{4-}$ anion. The solution and solid-state structures of the ditin anions will be reported in a subsequent paper.[15] The present paper reports the synthesis and the structural characterization by ^{119}Sn and ^{77}Se NMR spectroscopy, X-ray crystallography, and Raman spectroscopy of the $Sn_4Se_{10}^{4-}$ anion, which represents the first example of an adamantanoid cage containing only tin and a chalcogen and extends the series of isoelectronic Group 14 adamantanoid structures. The Raman spectrum of the $SnSe_4^{4-}$ anion in $(Na^+)_4SnSe_4^{4-}\cdot 2en$[16] is also reported for the first time and compared with those of $Sn_4Se_{10}^{4-}$ and related isoelectronic and isovalent species.

Results and Discussion

Synthesis of $Sn_4Se_{10}^{4-}$ and Structural Characterization by X-ray Crystallography. The experimental approach involved the synthesis of the ternary alloy $KSn_{0.67}Se_{1.93}$ by fusion of the elements followed by extraction of the powdered alloy in en and liquid NH_3 in the presence of a nonstoichiometric amount of 2,2,2-crypt with respect to K^+, where K^+:2,2,2-crypt = 1.00:0.42. Single crystals were isolated from an en solution upon addition of THF.

Details of the data collection parameters and other crystallographic information are given in Table 1. The final atomic coordinates and the equivalent isotropic thermal parameters for the Sn and Se atoms are summarized in Table 2. The most significant bond distances and angles in the $Sn_4Se_{10}^{4-}$ anion are given in Table 3.

The structures of the four crystallographically independent 2,2,2-crypt-K^+ cations are similar to those determined previously for symmetry unconstrained units in $K^+(2,2,2\text{-crypt-}K^+)_3Pb_9^{4-}$ [17] and $(2,2,2\text{-crypt-}K^+)_2Sn_2Se_3^{2-}$ [18] with average K···O and K···N distances of 2.829(11) and 2.963(7) Å, respectively. A complete list of bond distances and angles in the 2,2,2-crypt-K^+ cations is given in the supplementary material, Table S3.

The crystal structure consists of well-separated 2,2,2-crypt-K^+ cations and $Sn_4Se_{10}^{4-}$ anions. The most interesting aspect

[⊗] Abstract published in *Advance ACS Abstracts,* November 1, 1995.

(1) Dean, P. A. W.; Manivannan, V. *Inorg. Chem.* **1990**, *29*, 2997.
(2) Vittal, J. J.; Dean, P. A. W.; Payne, N. C. *Can. J. Chem.* **1992**, *70*, 792.
(3) Dean, P. A. W.; Vittal, J. J.; Wu, Y. *Inorg. Chem.* **1994**, *33*, 2180.
(4) Krebs, B.; Voelker, D.; Stiller, K. O. *Inorg. Chim. Acta* **1992**, *65*, L101.
(5) Ribes, M.; Olivier-Fourcade, J.; Philippot, E.; Maurin, M. *J. Solid State Chem.* **1973**, *8*, 195.
(6) Pohl, S.; Krebs, B. *Z. Anorg. Allg. Chem.* **1976**, *424*, 265.
(7) Eulenberger, G. *Acta Crystallogr.* **1976**, *B32*, 3059.
(8) Sheldrick, W. S.; Schaaf, B. *Z. Naturforsch.* **1994**, *49b*, 655.
(9) Eulenberger, G. *Z. Naturforsch.* **1981**, *36b*, 521.
(10) Dhingra, S. S.; Haushalter, R. C. *Polyhedron* **1994**, *13*, 2775.

0020-1669/95/1334-6265$09.00/0

Table 1. Summary of Crystal Data and Refinement Results for $(2,2,2\text{-crypt-}K^+)_4Sn_4Se_{10}^{4-}$

chemical formula $C_{72}H_{144}K_4N_8O_{24}Se_{10}Sn_4$	formula weight 2926.7
$a = 14.769(2)$ Å	space group $P\bar{1}$ (No. 2)
$b = 15.580(1)$ Å	$T = 24$ °C
$c = 26.275(4)$ Å	$\lambda = 0.71073$ Å
$\alpha = 79.19(1)°$	$\rho_{calcd} = 1.644$ g cm^{-3}
$\beta = 85.65(1)°$	$\mu = 41.14$ cm^{-1}
$\gamma = 85.870(8)°$	$R_1{}^a = 0.0701$
$V = 5911(1)$ Å^3	$wR_2{}^b = 0.2024$
$Z = 2$	

$^a R_1 = \sum||F_o| - |F_c||/\sum|F_o|$. $^b wR_2 = [\sum[w(F_o^2 - F_c^2)^2]/\sum w(F_o^2)^2]^{1/2}$.

Table 2. Atomic Coordinates ($\times 10^4$) and Equivalent Isotropic Displacement Parameters (Å$^2 \times 10^3$) for the Sn and Se atoms in $(2,2,2\text{-crypt-}K^+)_4Sn_4Se_{10}^{4-}$

	x	y	z	U(eq)[a]
Sn(1)	6891(1)	3524(1)	1893(1)	49(1)
Sn(2)	7362(1)	2408(1)	3408(1)	48(1)
Sn(3)	5326(1)	1516(1)	2693(1)	43(1)
Sn(4)	8017(1)	1011(1)	2238(1)	39(1)
Se(1)	5322(1)	2928(1)	2033(1)	63(1)
Se(2)	7354(1)	3831(1)	2747(1)	66(1)
Se(3)	8029(1)	2411(1)	1552(1)	57(1)
Se(4)	8554(1)	1338(1)	3077(1)	50(1)
Se(5)	5814(1)	1743(1)	3567(1)	53(1)
Se(6)	6451(1)	378(1)	2384(1)	48(1)
Se(7)	7746(1)	2753(1)	4223(1)	83(1)
Se(8)	3768(1)	1109(1)	2750(1)	70(1)
Se(9)	9038(1)	−112(1)	1936(1)	55(1)
Se(10)	6793(1)	4907(1)	1286(1)	77(1)

[a] U(eq) is defined as one-third of the trace of the orthogonalized U_{ij} tensor.

Table 3. Bond Lengths (Å) and Bond Angles (deg) for the $Sn_4Se_{10}^{4-}$ Anion in $(2,2,2\text{-crypt-}K^+)_4Sn_4Se_{10}^{4-}$

Bond Lengths (Å)			
Sn(1)-Se(10)	2.431(2)	Sn(1)-Se(1)	2.534(2)
Sn(1)-Se(2)	2.533(2)	Sn(1)-Se(3)	2.562(2)
Sn(2)-Se(7)	2.418(2)	Sn(2)-Se(2)	2.548(2)
Sn(2)-Se(5)	2.551(2)	Sn(2)-Se(4)	2.555(2)
Sn(3)-Se(8)	2.416(2)	Sn(3)-Se(1)	2.533(2)
Sn(3)-Se(6)	2.545(2)	Sn(3)-Se(5)	2.551(2)
Sn(4)-Se(9)	2.433(2)	Sn(4)-Se(4)	2.550(2)
Sn(4)-Se(6)	2.553(2)	Sn(4)-Se(3)	2.557(2)
Bond Angles (deg)			
Se(10)-Sn(1)-Se(1)	107.98(7)	Se(10)-Sn(1)-Se(2)	107.85(6)
Se(1)-Sn(1)-Se(2)	108.67(7)	Se(10)-Sn(1)-Se(3)	111.77(7)
Se(1)-Sn(1)-Se(3)	109.80(6)	Se(2)-Sn(1)-Se(3)	110.66(7)
Se(7)-Sn(2)-Se(2)	107.07(7)	Se(7)-Sn(2)-Se(5)	107.19(6)
Se(2)-Sn(2)-Se(5)	113.06(6)	Se(7)-Sn(2)-Se(4)	111.50(7)
Se(2)-Sn(2)-Se(4)	107.62(6)	Se(5)-Sn(2)-Se(4)	110.41(6)
Se(8)-Sn(3)-Se(1)	103.55(7)	Se(8)-Sn(3)-Se(6)	112.96(6)
Se(1)-Sn(3)-Se(6)	110.08(6)	Se(8)-Sn(3)-Se(5)	111.79(6)
Se(1)-Sn(3)-Se(5)	111.36(6)	Se(6)-Sn(3)-Se(5)	107.16(6)
Se(9)-Sn(4)-Se(4)	109.60(6)	Se(9)-Sn(4)-Se(6)	105.68(6)
Se(4)-Sn(4)-Se(6)	111.31(5)	Se(9)-Sn(4)-Se(3)	109.41(6)
Se(4)-Sn(4)-Se(3)	108.80(6)	Se(6)-Sn(4)-Se(3)	111.98(6)
Sn(1)-Se(1)-Sn(3)	110.80(6)	Sn(1)-Se(2)-Sn(2)	108.58(6)
Sn(4)-Se(3)-Sn(1)	106.74(6)	Sn(4)-Se(4)-Sn(2)	107.25(6)
Sn(3)-Se(5)-Sn(2)	107.60(6)	Sn(3)-Se(6)-Sn(4)	108.11(5)

of the structure is the adamantanoid geometry of the anion with approximate T_d symmetry in which the tin atoms occupy the bridgehead positions and the selenium atoms occupy the bridging and terminal sites (Figure 1). The Se−Sn−Se bond angles range from 103.55(7)° to 113.06(6)°, so that the $Sn_4Se_{10}^{4-}$ anion can be described as composed of four nearly tetrahedral Sn^{IV} centers to which are bonded four Se_t atoms and six Se_b atoms. The bond angles within the central Sn_4Se_6 core, $Se_b-Sn-Se_b$, are 110.08(6)° [range, 107.16(6)−113.06(6)°] and are slightly larger than those involving terminal bonds, $Se_t-Sn-Se_b$, which are 108.86(6)° [range, 103.55(7)−112.96(6)°], a trend common to all known $M_4Ch_{10}^{4-}$ adamantanoid anions.[4-10] The $Se_t-Sn-Se_b$ angles are close to the ideal tetrahedral angles observed in $SnSe_4^{4-}$ [109.50(5)° in Na_4SnSe_4 and 109.47(3)° in K_4SnSe_4],[19] and the $Se_b-Sn-Se_b$ angles are comparable to those in other systems containing the Sn_4Se_6 core, i.e., $(CH_3)_4Sn_4Se_6$ [110.13(4)−115.19(4)°][12] and $\{Cp(CO)_2Fe\}_4Sn_4Se_6$ [108.8(1)−111.8(1)°].[13] The average $Sn-Se_b-Sn$ angle is 108.18(6)° [range, 106.74(6)−110.80(6)°] and is comparable to those in $(CH_3)_4Sn_4Se_6$ [102.13(4)−103.75(4)°] and $\{Cp(CO)_2Fe\}_4Sn_4Se_6$ [107.3(1)−109.0(1)°].

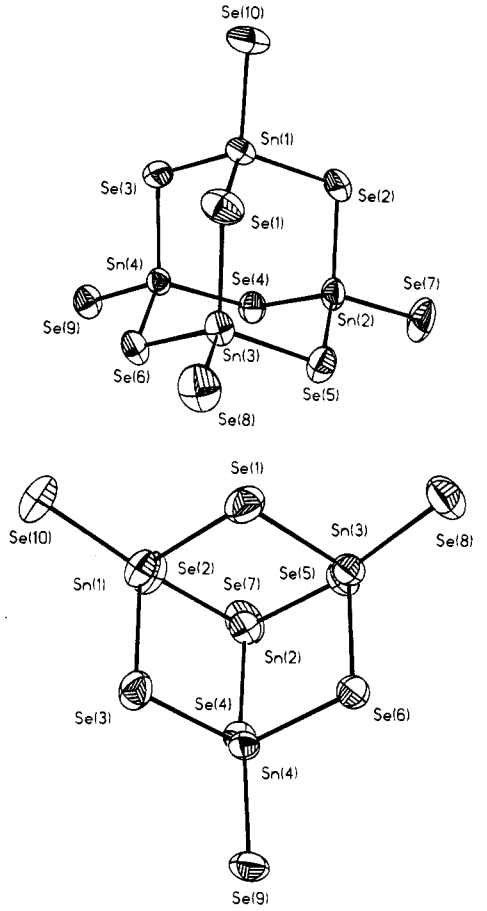

Figure 1. Two ORTEP views of the $Sn_4Se_{10}^{4-}$ anion in $(2,2,2\text{-crypt-}K^+)_4Sn_4Se_{10}^{4-}$. Thermal ellipsoids are drawn at the 50% probability level.

As already observed in other adamantanoid structures of Group 14, i.e., $Si_4S_{10}^{4-}$ [5] and $Ge_4Ch_{10}^{4-}$ (Ch = S, Se, Te),[5-10] the $Sn-Se_t$ bond lengths [range, 2.416(2)−2.433(2) Å] are shorter than the $Sn-Se_b$ bond lengths [range, 2.533(2)−2.557(2) Å]. This trend has also been observed in the related $Sn_2Ch_6^{4-}$ (Ch = S,[20] Se,[21] Te [22,23]) and $Sn_2Te_7^{4-}$ [24] anions and in the adamantanoid structures of Group 13, i.e., $Ga_4S_{10}^{8-}$ and

(11) Dörfelt, C.; Janeck, A.; Kobelt, D.; Paulus, E. F.; Scherer, H. *J. Organomet. Chem.* **1968**, *14*, P22.
(12) Blecher, A.; Drager, M.; Mathiasch, B. *Z. Naturforsch.* **1981**, *36b*, 1361.
(13) Mertzweiler, K.; Weisse, L. *Z. Naturforsch.* **1990**, *45b*, 971.
(14) Merzweiler, K.; Kraus, H. *Z. Naturforsch.* **1994**, *49b*, 621.
(15) Campbell, J.; Gerken, M.; Mercier, H. P. A.; Pirani, A. M.; Schrobilgen, G. J. *Inorg. Chem.*, in press.
(16) The addition of THF to an en extract of the alloy $NaSn_{0.4}Se$ (final en:THF = 1:2 v/v) gave rise to yellow-orange needle-shaped crystals of $(Na^+)_4SnSe_4^{4-}\cdot$ 2en. A data set was obtained for one of these crystals, but the structure could only be partially solved in the space group $P4_32_12$ because two en solvent molecules and a cation were highly disordered. The tetrahedral geometry of the anion could, however, be refined (Sn−Se distance, 2.52 Å).

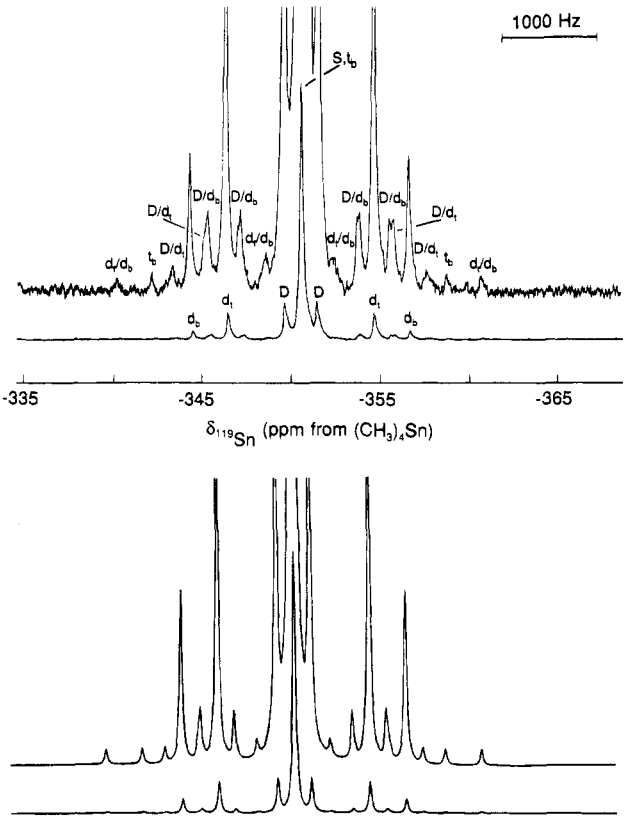

Figure 2. Observed (upper trace) and simulated (lower trace) ^{119}Sn NMR spectrum (185.504 MHz) of $Sn_4Se_{10}^{4-}$ in liquid NH_3 at −50 °C. The symbols used to label the peaks are defined in Table 5 and in the text.

$In_4Ch_{10}^{8-}$ (Ch = S, Se).[4] However, the difference between M−Ch_t and M−Ch_b is more pronounced in $Sn_4Se_{10}^{4-}$, indicating stronger bonding to the terminal chalcogen atoms (see **Raman Spectra of the $SnSe_4^{4-}$ and $Sn_4Se_{10}^{4-}$ Anions**), but longer and more polar M-Ch_t bonds have been observed in the Group 13 analogues by virtue of the higher charge on the terminal chalcogen atoms. The Sn−Se_t bond lengths are slightly shorter than those found in the tetrahedral $SnSe_4^{4-}$ anion [2.523(1) Å in Na_4SnSe_4 and 2.510(1) Å in K_4SnSe_4], and the Sn−Se_b bond lengths are comparable to those in $(CH_3)_4Sn_4Se_6$ [2.513(1)−2.541(1) Å] and in $\{Cp(CO)_2Fe\}_4Sn_4Se_6$ [2.524(5)−2.554(4) Å]. The $Sn^{IV}\cdots Sn^{IV}$ distances range from 4.108 to 4.173 Å and are significantly longer than the corresponding distance observed in $Sn_2Se_6^{4-}$ [3.518 Å].

The Sn−Se_t, Sn−Se_b bond lengths and the Sn−Se_b−Sn, Se_b−Sn−Se_b bond angles within the Sn_4Se_6 core are comparable to those found in other compounds in which the environment about tin atoms is also approximately tetrahedral and that about the chalcogens is bent: $K_4Sn_3Se_8$, 2.473(1) Å, 2.520(1) Å and 85.67(4)°, 104.85(6)°;[25] $Rb_4Sn_2Se_6$, 2.462(4) Å, 2.594(5) Å, and 85.4(1)°, 94.6(1)°.[21]

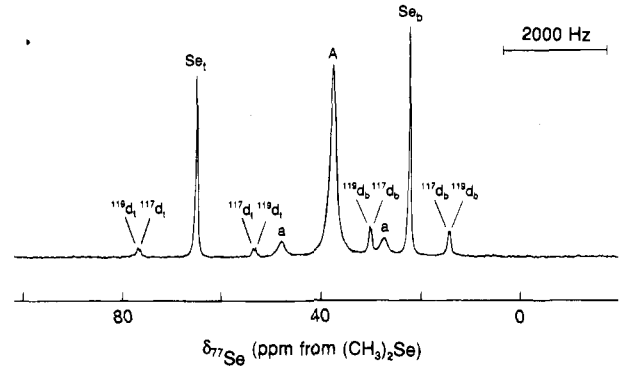

Figure 3. ^{77}Se NMR spectrum (95.383 MHz) of $Sn_4Se_{10}^{4-}$ in en at 0 °C. Se_t denotes terminal selenium atoms; Se_b denotes bridging selenium atoms; $^{117,119}d_t$ and $^{117,119}d_b$ denote satellite doublets arising from $^1J(^{117,119}Sn-^{77}Se_t)$ and $^1J(^{117,119}Sn-^{77}Se_b)$, respectively. (A denotes the terminal selenium environment of $Sn_2Se_6^{4-}$ and a denotes the unresolved ^{117}Sn and ^{119}Sn satellites; see ref. 15.)

Solution Characterization of $Sn_4Se_{10}^{4-}$ by ^{77}Se and ^{119}Sn NMR Spectroscopy. The $Sn_4Se_{10}^{4-}$ anion was identified in solution by natural abundance ^{77}Se and ^{119}Sn NMR spectroscopy.[26] The experimental ^{119}Sn and ^{77}Se NMR spectra and the simulated ^{119}Sn NMR spectrum are depicted in Figures 2 and 3. The chemical shifts and spin−spin coupling constants (scalar, J; reduced, K;[27] and relativistically corrected reduced, K_{RC}[28]) are summarized in Table 4 together with the observed and calculated satellite/central (I_S/I_C) intensity ratios[18,28] for the Sn and Se environments of the anion. The number of observed environments, satellite doublet spacings corresponding to $^1J(^{119}Sn-^{77}Se)$ and $^2J(^{119}Sn-^{117}Sn)$, and I_S/I_C intensity ratios are consistent with the crystal structure of $Sn_4Se_{10}^{4-}$ and indicate that the solid-state molecular structure of the anion is retained in solution.

In addition to the resonances associated with the $SnSe_3^{2-}$ (−299.5 ppm, 1.0%), $Sn_2Se_6^{4-}$ (−491.6 ppm, 57.0%), and $Sn_2Se_7^{4-}$ (−328.4 ppm, 15.0%) anions, the ^{119}Sn NMR spectrum (−50 °C) consisted of a singlet (−350.1 ppm, 27.0%) flanked by two sets of symmetric ^{77}Se satellites (d_t, 2274 Hz; d_b, 1536 Hz) in a 1.0:3.2 peak area ratio, indicating coupling to two chemically inequivalent selenium environments (Figure 2). Satellites corresponding to $^2J(^{119}Sn-^{117}Sn)$ were also observed in the ^{119}Sn NMR spectrum and their spacing (342 Hz) is similar to $^2J(^{119}Sn-^{117}Sn)$ observed for the $Sn_2Se_7^{4-}$ anion (302 Hz).[15] Comparable $^2J(^{119}Sn-^{117}Sn)$ couplings of 205, 235, and 263 Hz have been observed for the solution structures of the dimethyltin(IV) chalcogenides $[(CH_3)_2SnCh]_3$ (Ch = S, Se, Te), respectively.[29] In addition, several weaker satellites were observed in the ^{119}Sn NMR spectrum of $Sn_4Se_{10}^{4-}$ (Figure 2) and their assignments are discussed below.

The ^{119}Sn NMR spectrum of the $Sn_4Se_{10}^{4-}$ anion was simulated by using the natural abundances of the spin-$^1/_2$ nuclides ^{117}Sn, ^{119}Sn, and ^{77}Se;[26] the values of the observed coupling constants; and the probabilities of the most abundant

(17) Campbell, J.; Dixon, D. A.; Mercier, H. P. A.; Schrobilgen, G. J. *Inorg. Chem.* **1995**, *34*, 5798.
(18) Björgvinsson, M.; Mercier, H. P. A.; Mitchell, K. M.; Schrobilgen, G. J.; Strohe, G. *Inorg. Chem.* **1993**, *32*, 6046.
(19) Klepp, K. O. *Z. Naturforsch.* **1992**, *47b*, 411.
(20) Krebs, B.; Müller, H. *Z. Anorg. Allg. Chem.* **1983**, *496*, 47.
(21) Sheldrick, W. S.; Schaaf, B. *Z. Anorg. Chem.* **1994**, *620*, 1041.
(22) Ansari, M. A.; Bollinger, J. C.; Ibers, J. A. *Inorg. Chem.* **1993**, *32*, 231.
(23) Huffman, J. C.; Haushalter, J. P.; Shenoy, G. K.; Haushalter, R. C. *Inorg. Chem.* **1984**, *23*, 2312.
(24) Brinkmann, C.; Eisenmann, B.; Schäfer, H. *Mat. Res. Bull.* **1985**, *20*, 299.
(25) Sheldrick, W. S. *Z. Naturforsch.* **1988**, *43b*, 249.
(26) Mason, J. In *Multinuclear NMR*; Plenum Press: New York, 1987; Appendix, pp 626−627.
(27) The reduced coupling constant, K_{AB}, is defined as $(4\pi^2/h\gamma_A\gamma_B)\cdot J_{AB}$, where h is Planck's constant and γ_A and γ_B are the gyromagnetic ratios of the spin-coupled nuclei A and B; see: Pople, J. A.; Santry, D. P. *Mol. Phys.* **1964**, *8*, 1.
(28) A detailed discussion of the relativistically corrected reduced coupling constants, K_{RC}, may be found in: (a) Björgvinsson, M.; Sawyer, J. F.; Schrobilgen, G. J. *Inorg. Chem.* **1987**, *26*, 741. (b) Burns, R. C.; Devereux, L. A.; Granger, P.; Schrobilgen, G. *Inorg. Chem.* **1985**, *24*, 2615.
(29) Gay, I. D.; Jones, C. H. W.; Sharma, R. D. *J. Magn. Reson.* **1989**, *84*, 501.

Table 4. Chemical Shifts, Spin−Spin Coupling Constants, and Relative Satellite Intensities for the $Sn_4Se_{10}^{4-}$ Anion

chemical shift[a], ppm		spin−spin coupling constants							
		J, Hz		K, $T^2 J^{-1} \times 10^{20}$		K_{RC}, $T^2 J^{-1} \times 10^{20}$		$100 \times I_S/I_C$[b]	
^{119}Sn	^{77}Se[c]	$^{119}Sn-^{77}Se$	$^{119}Sn-^{117}Sn$	Sn−Se	Sn−Sn	Sn−Se	Sn−Sn	Sn	Se
−350.1[d]	30.7(t)	2274	342	263.7	21.8	160.2	10.4	3.5(4.1)	
	7.1(b)	1536		178.1		108.2		10.4(12.2)	
−359.3[e]	65.0(t)	2276	333	263.9	20.6	160.4	10.2		8.5(9.6)
	22.2(b)	1532		177.7		107.9			17.5(19.2)

[a] Satellites were resolved in the ^{119}Sn NMR spectrum at both −50 and 0 °C; however, the ^{119}Sn NMR spectrum obtained at 0 °C was broadened and the ^{77}Se spectrum obtained at −50 °C contained a number of overlapping peaks which precluded accurate satellite assignments and I_S/I_C calculations. Consequently, the discussion of the NMR parameters (see Text) refers to those obtained at −50 (^{119}Sn) and 0 (^{77}Se) °C. [b] Calculated values are given in parentheses. [c] The symbols, t and b, refer to terminal and bridging selenium atoms, respectively. [d] Recorded in liquid NH_3 at −50 °C. [e] Recorded in en at 0 °C.

Table 5. Natural Abundance Isotopomers and Subspectra Used To Simulate the ^{119}Sn NMR Spectrum of the $Sn_4Se_{10}^{4-}$ Anion

$^{119}Sn_x{}^{117}Sn_y Sn_{4-x-y}{}^{77}Se_z Se_{10-z}^{4-}$[a]			abundance,[b] %	multiplicity of subspectrum[c]
x	y	z		
1	0	0	9.183	S
1	0	1	4.531	S
			2.265	d_b
			0.755	d_t
1	0	2	1.223	S
			0.524	d_t
			0.524	d_b
			0.262	d_t/d_b
			0.262	t_b
1	1	0	2.499	D
1	1	1	1.233	D
			0.617	D/d_t
			0.206	D/d_b
1	1	2	0.318	D/d_b
			0.283	D
			0.106	D/d_t
2	0	0	2.828	S
2	0	1	1.163	d_b
			0.698	S
			0.465	d_t
2	0	2	0.349	d_b
			0.163	d_t
			0.140	d_t/d_b
			0.140	t_b
			0.070	S
2	1	0	0.513	D
2	1	1	0.195	D
			0.162	D/d_b
			0.065	D/d_t
3	0	0	0.290	S
3	0	1	0.143	d_b
			0.072	d_t
			0.024	S

[a] Low abundance isotopomers having multiplet lines which are too weak to be observed in the spectrum are not considered. [b] Natural abundances of spin-1/2 nuclides used to calculate isotopomer abundances were taken from ref 26; ^{77}Se, 7.58%; ^{117}Sn, 7.61%; and ^{119}Sn, 8.58%. The natural abundance of ^{115}Sn, 0.35%, is too low to contribute detectable isotopomer subspectra and is combined with the spinless tin nuclides. [c] S denotes a singlet, D denotes a DOUBLET arising from $^2J(^{119}Sn-^{117}Sn)$, d_t and d_b denote doublets arising from $^1J(^{119}Sn-^{77}Se_t)$ and $^1J(^{119}Sn-^{77}Se_b)$, respectively, and t_b denotes a triplet arising from $^1J(^{119}Sn-^{77}Se_b)$. The symbols, D/d_t and D/d_b, denote DOUBLET-of-doublets involving a DOUBLET arising from $^2J(^{119}Sn-^{117}Sn)$, which, in turn, is split into a doublet by either $^1J(^{119}Sn-^{77}Se_t)$ or $^1J(^{119}Sn-^{77}Se_b)$, respectively. The doublet-of-doublets arising from $^1J(^{119}Sn-^{77}Se_t)$ and $^1J(^{119}Sn-^{77}Se_b)$ is denoted by d_t/d_b.

(≥0.024%) isotopic isomers (isotopomers) contributing significant first-order subspectra to the experimental ^{119}Sn NMR spectrum. Table 5 lists the isotopomer abundances and multiplicities used to simulate the ^{119}Sn NMR spectrum. The resulting simulation (Figure 2) is in excellent agreement with the experimental spectrum and accounts for all the observed satellite peaks. A singlet (S) is observed for the isotopomers in which no ^{77}Se atoms are directly bonded to spin-active Sn atoms, namely, $^{119}Sn_xSn_{4-x}{}^{77}Se_zSe_{10-z}^{4-}$ ($x = 1-3$; $z = 0-2$). When one terminal or one bridging ^{77}Se atom is directly bonded to a spin-active Sn atom, a doublet (d_t or d_b) results which is symmetrically disposed about the central singlet (S) at a spacing corresponding to $^1J(^{119}Sn-^{77}Se_t)$ or $^1J(^{119}Sn-^{77}Se_b)$, respectively. The isotopomers, $^{119}Sn_x{}^{117}SnSn_{3-x}{}^{77}Se_zSe_{10-z}^{4-}$ ($x = 1, 2$; $z = 0-2$), give rise to a DOUBLET (D) arising from $^2J(^{119}Sn-^{117}Sn)$ coupling when no ^{77}Se atoms are bonded to ^{119}Sn atoms. The presence of a ^{77}Se atom in a terminal or a bridging position directly bonded to a ^{119}Sn atom gives rise to a DOUBLET-of-doublets (D/d_t or D/d_b) whose transitions are symmetrically disposed about the binomial doublets d_t or d_b, respectively (Figure 2). The lowest abundance isotopomers that are detectable are $^{119}Sn_xSn_{4-x}{}^{77}Se_2Se_8$ ($x = 1, 2$) and give rise to either a 1:2:1 triplet (t_b), when both ^{77}Se atoms are bridged to at least one ^{119}Sn atom, or a doublet-of-doublets (d_t/d_b), when one ^{77}Se atom is terminal and the other is bridging and directly bonded to at least one ^{119}Sn atom. The central transition of the triplet lies under the central singlet (S), while the outer two transitions are observed at a spacing corresponding to $^1J(^{119}Sn-^{77}Se_b)$ on either side of the central singlet. The transitions of the doublet-of-doublets are observed symmetrically disposed about the central singlet.

Assignments of $^1J(^{119}Sn-^{77}Se)$ couplings observed in the ^{119}Sn NMR spectrum were confirmed by observing the $^1J(^{77}Se-^{119}Sn)$ couplings in the ^{77}Se NMR spectrum. The ^{77}Se signals corresponding to the two environments were observed in a 4.0:6.3 peak area ratio at 65.0 and 22.2 ppm, respectively (Figure 3). The I_S/I_C peak area ratios indicated that the two selenium environments were coupled to one and two tin atoms, respectively, and are consistent with the adamantanoid $Sn_4Se_{10}^{4-}$ structure.

As expected, $^1J(^{119}Sn-^{77}Se_t)$ was found to be larger than $^1J(^{119}Sn-^{77}Se_b)$ and indicates a higher bond order for the Sn−Se_t bond than for the Sn−Se_b bond and is consistent with the shorter Sn−Se_t bonds [average, 2.425(2) Å] and the longer Sn−Se_b bonds [average, 2.548(2) Å] observed for the $Sn_4Se_{10}^{4-}$ anion. The magnitude of $^1J(^{119}Sn-^{77}Se_b)$, 1536 Hz, is similar to those determined for $Sn_2Se_7^{4-}$ (monoseleno-bridge, Se_{mb}, 1134 Hz; diseleno-bridge, Se_{db}, 1324 Hz)[15] and the Se-bridged compound $[(CH_3)_2SnSe]_3$ (1219 Hz),[29] and the $^1J(^{119}Sn-^{77}Se_t)$ value of 2274 Hz agrees with analogous values determined for $SnSe_3^{2-}$ (2051 Hz),[28b] $Sn_2Se_6^{4-}$ (2005 Hz), and $Sn_2Se_7^{4-}$ (2037 Hz).[15]

In the $Sn_4Se_{10}^{4-}$ anion, the ^{77}Se NMR signal corresponding to the terminal selenium, Se_t, environment was found to be more deshielded (65.0 ppm) than the signal associated with the bridging selenium, Se_b, environment (22.2 ppm). The small chemical shift difference (Δ) between the two chalcogen

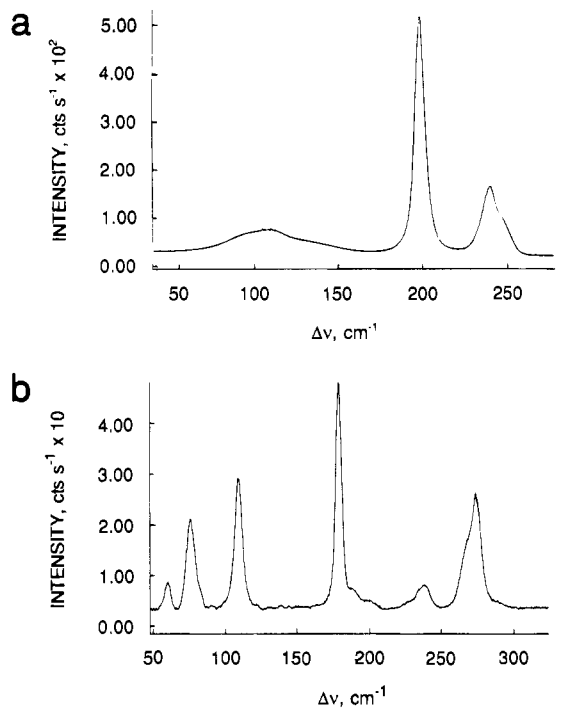

Figure 4. Raman spectrum of microcrystalline (a) $SnSe_4^{4-}$ in $(Na^+)_4SnSe_4^{4-}\cdot 2en$ and (b) $Sn_4Se_{10}^{4-}$ in $(2,2,2\text{-crypt-}K^+)_4Sn_4Se_{10}^{4-}$ recorded in glass capillaries at room temperature, using 514.5-nm excitation.

environments in $Sn_4Se_{10}^{4-}$ (42.8 ppm) can be rationalized by using the rule of topological charge stabilization.[30] This rule has been applied to adamantanoid structures, M_4X_6, as well as to bridgehead-substituted adamantanoids, $M_4X_6R_4$, and when extended to the isostructural $Sn_4Se_{10}^{4-}$ anion predicts that the 4− charge is distributed over both the Se_t and Se_b atoms but is concentrated on the terminal Se atoms. This gives rise to a smaller Δ, which contrasts with the larger values observed for the dimeric $Sn_2Ch_6^{4-}$ and $Sn_2Ch_7^{4-}$ (Ch = Se, Te) anions where the 4− charge is primarily localized on the terminal atoms [$Sn_2Ch_6^{4-}$, Se, 257.5 ppm, Te, 547 ppm; $Sn_2Se_7^{4-}$, 27.9 ppm, $\delta(Ch_t) - \delta(Ch_{db})$, 174.9 ppm; $Sn_2Te_7^{4-}$, 228 ppm, $\delta(Ch_t) - \delta(Ch_{db})$, 199 ppm].[15] However, for the $Sn_2Te_7^{4-}$ anion, the order was found to be $\delta(Te_{mb}) > \delta(Te_{db})$, which is the reverse of the order predicted by charge topology arguments and may attributed to shielding anisotropy,[31] which may also account for the order, $\delta(Se_b) < \delta(Se_t)$, observed for the $Sn_4Se_{10}^{4-}$ anion. However, in the absence of a knowledge of the ^{77}Se and ^{125}Te shielding tensors, the apparent anomalies in the ^{77}Se and ^{125}Te shielding trends are presently not fully understood.

Raman Spectra of the $SnSe_4^{4-}$ and $Sn_4Se_{10}^{4-}$ Anions. The solid-state Raman spectra of $(Na^+)_4SnSe_4^{4-}\cdot 2en$[16] and $(2,2,2\text{-crypt-}K^+)_4Sn_4Se_{10}^{4-}$ are shown in Figure 4 and the Raman frequencies and their assignments are listed in Table 6. Assignments for the en solvent molecule and for the 2,2,2-crypt-K^+ cation were made by comparison with values reported for the solid-state Raman spectra of en[34] and for $(2,2,2\text{-crypt-}K^+)I^-$.[35] No en bands are found within the frequency window containing the $SnSe_4^{4-}$ bands. The Raman spectrum of $(2,2,2\text{-crypt-}K^+)I^-$ displayed several very weak, broad bands in the 50−350-cm^{-1} region. The most intense 2,2,2-crypt-K^+ band at 135 cm^{-1}, which does not overlap with any $Sn_4Se_{10}^{4-}$ anion bands, was too weak to be observed in the Raman spectrum of $(2,2,2\text{-crypt-}K^+)_4Sn_4Se_{10}^{4-}$.

Table 6. Raman Frequencies and Assignments for $SnSe_4^{4-}$ in $(Na^+)_4SnSe_4^{4-}\cdot 2en$, $Sn_4Se_{10}^{4-}$ in $(2,2,2\text{-crypt-}K^+)_4Sn_4Se_{10}^{4-}$, and the related SnS_4^{4-} and $Ge_4S_{10}^{4-}$ Anions

frequency, cm^{-1}		assignments	frequency, cm^{-1}		assignments
SnS_4^{4-} [a]	$SnSe_4^{4-}$		$Ge_4S_{10}^{4-}$ [b]	$Sn_4Se_{10}^{4-}$	
150[c]	109(10)	$\nu_2(E)$	112(5)	59(12)	$\nu_{15}(T_2)$
170[c]	136(5)	$\nu_4(T_2)$	148(14)	74(40)	$\nu_{14}(T_2)$
348(st)	199(100)	$\nu_1(A_1)$	160[c]	81 sh	$\nu_5(E)$
344(m)	239(29), 247 sh	$\nu_3(T_2)$	193(29)	108(58)	$\nu_3(A_1)$
			210(2)		$\nu_{13}(T_2)$
			346(100)	178(100)	$\nu_2(A_1)$
			378(4)	188(9), 200(4)	$\nu_{12}(T_2)$
			405(10)	227(4), 238(11)	$\nu_{11}(T_2)$
			446sh	268sh	$\nu_{10}(T_2)$
			457(22)	274(51)	$\nu_1(A_1)$
			410[c]	290sh	$\nu_4(E)$

[a] Reference 32. [b] Reference 33. [c] Obtained from a normal coordinate analysis.

$SnSe_4^{4-}$. The vibrational modes of the $SnSe_4^{4-}$ anion were assigned under T_d point symmetry and belong to the irreducible representation $\Gamma = A_1 + E + 2T_2$. A total of four vibrational bands are expected, $\nu_1(A_1)$, $\nu_2(E)$, $\nu_3(T_2)$, and $\nu_4(T_2)$, all of which are Raman active, while the $\nu_3(T_2)$ and $\nu_4(T_2)$ bands are also infrared active. Assignments were made by analogy with the isoelectronic species $CdBr_4^{2-}$,[36] $InBr_4^-$,[37] $SnBr_4$,[38] and $SbBr_4^+$[39] as well as with the isovalent SnS_4^{4-} anion.[32] Among the four bands expected for SnS_4^{4-}, only the two high-frequency modes, $\nu_1(A_1)$ and $\nu_2(E)$, were observed. Their assignment was confirmed by using polarization measurements and normal coordinate analyses, which also calculated the frequencies for $\nu_3(T_2)$ and $\nu_4(T_2)$.

Two sharp and two broad bands were observed in the Raman spectrum of $SnSe_4^{4-}$. The most intense peak (199 cm^{-1}) was assigned to the totally symmetric Sn−Se stretch, $\nu_1(A_1)$. A peak at 239 cm^{-1} was assigned to the asymmetric Sn−Se stretch, $\nu_3(T_2)$, and was split due to site symmetry lowering in the crystal (C_2 crystal site symmetry). The broad bands at lower wavenumbers (109 and 136 cm^{-1}) were assigned to the partially overlapping antisymmetric Se−Sn−Se bends, $\nu_2(E)$ and $\nu_4(T_2)$, respectively. As expected, the stretching frequencies decrease from SnS_4^{4-} to $SnSe_4^{4-}$ in accord with the reduced mass effect

(30) Gimarc, B. M.; Ott, J. J. *J. Am. Chem. Soc.* **1986**, *108*, 4298.
(31) Mason, J. In *Multinuclear NMR*; Plenum Press: New York, 1987; Chapter 5, p 149.
(32) Pohl, S.; Schiwy, W.; Weinstock, N.; Krebs, B. *Z. Naturforsh.* **1973**, *28b*, 565.
(33) Müller, A.; Cyvin, B. N.; Cyvin, S. J.; Pohl, S.; Krebs, B. *Spectrochim. Acta* **1976**, *32A*, 67.
(34) Giorgini, M. G.; Pelletti, M. R.; Paliani, G.; Cataliotti, R. S. *J. Raman Spectrosc.* **1983**, *14*, 16.
(35) The solid-state Raman spectrum of microcrystalline (2,2,2,-crypt-K^+)-I^- was recorded at room temperature under the same conditions used to record the spectrum of $(2,2,2\text{-crypt-}K^+)_4Sn_4Se_{10}^{4-}$. Only four weak Raman modes could be observed in the range 50−350 cm^{-1}, i.e., 94-(33), 135(100), 175(42), and 216(17) cm^{-1}.
(36) Goggin, P. L.; Goodfellow, R. J.; Kessler, K. *J. Chem. Soc., Dalton Trans.* **1977**, 1914.
(37) Woodward, L. A.; Bill, P. T. *J. Chem. Soc.* **1955**, 1699.
(38) Clark, R. J. H.; Mitchell, P. D. *J. Chem. Soc., Faraday Trans.* **1975**, *71(2)*, 515.
(39) Casteel, W. J.; Kolb, P.; LeBlond, N.; Mercier, H. P. A.; Schrobilgen, G. J. *Inorg. Chem.*, in press.
(40) Brand, P.; Sackmann, H. *Acta Crystallogr.* **1963**, *16*, 446.
(41) Beno, M. A.; Cox, D. D.; William, J. M.; Kwak, J. F. *Acta Crystallogr.* **1984**, *C40*, 1334.
(42) Khan, M. A.; Tuck, D. G. *Acta Crystallogr.* **1982**, *B38*, 803.
(43) Altermatt, D.; Arend, H.; Gramlich, V.; Niggli, A.; Petter, W. *Acta Crystallogr.* **1984**, *B40*, 347.
(44) Eisenmann, B.; Zagler, R. *Z. Naturforsch.* **1989**, *44B*, 249.
(45) Woodward, L. A.; Taylor, M. J. *J. Chem. Soc.* **1960**, 4473.
(46) Sanyal, N. K.; Panday, A. N.; Singh, H. S. *J. Mol. Spectrosc.* **1969**, *30*, 144.
(47) Mayer, H.; Mereiter, K. *Monatsh. Chem.* **1992**, *123*, 515.
(48) Jumas, J. C.; Philippot, E.; Vermot-Gaud-Daniel, F.; Ribes, M.; Maurin, M. *J. Solid State Chem.* **1975**, *14*, 319.

Table 7. Raman Frequencies and Bond Lengths for $SnSe_4^{4-}$, SnS_4^{4-}, and Isoelectronic Species

	frequency, cm^{-1}					M−X/Ch bond	
MX_4	$\nu_2(E)$	$\nu_4(T_2)$	$\nu_1(A_1)$	$\nu_3(T_2)$	ref	lengths, Å	ref
$SbBr_4^+$	76.2	92.1	234.4	304.9	39	2.385(2)	39
$SnBr_4$	59.4	85.9	222.1	284.0	38	2.40(3)	40
$InBr_4^-$	55	79	197	239	37	2.489(3), 2.479(3)	41, 42
$CdBr_4^{2-}$	49	75,61	161	177	36	2.560	43
$SbSe_4^{3-}$						2.459(4), 2.475(3)	44
$SnSe_4^{4-}$	109	136	199	247, 239	16	2.510(1), 2.523(1)	25
$SbCl_4^+$	121.5	139.4	395.6	450.7	39	2.221(3)	39
$SnCl_4$	95.2	126.1	369.1	408.2	38		
$InCl_4^-$	89	112	321	337	45	2.350(3)	42
$CdCl_4^{2-}$	84	98	261	249, 240	36		
SbS_4^{3-}	156	178	366	380	46	2.327(1)	47
SnS_4^{4-}	150[a]	170[a]	348	344	32	2.388(4), 2.396(3)	48

[a] Obtained from a normal coordinate analysis.

(Table 7), and the ordering, $\nu_3(T_2) > \nu_1(A_1)$ and $\nu_4(T_2) > \nu_2(E)$, follows trends observed for all tetrahedral, isoelectronic halogen compounds (Table 7). It should be pointed out, however, that in SnS_4^{4-}, $\nu_1(A_1)$ is slightly higher in frequency than $\nu_3(T_2)$.

The high negative charges of the SnS_4^{4-} and $SnSe_4^{4-}$ and the isoelectronic SbS_4^{3-} and $SbSe_4^{3-}$ anions should result in longer, more polar bonds and lower stretching frequencies than in the isoelectronic CdX_4^{2-}, InX_4^-, SnX_4, and SbX_4^+ (X = Cl, Br) species. Although the experimental M−X (M = In, Sn, Sb) and M′−Ch (M′ = Sn, Sb; Ch = S, Se) bond lengths generally show the expected increase with increasing negative charge over both isoelectronic series, i.e., $CdBr_4^{2-} > SnCh_4^{4-} > InX_4^- > SbCh_4^{3-} > SnX_4 > SbX_4^+$, the bond lengths and stretching frequencies of SbS_4^{3-} and $SnCh_4^{4-}$ are intermediate with respect to the isoelectronic halide series (Table 7). This is exemplified by the stretching modes of $SnSe_4^{4-}$, $\nu_1(A_1)$ and $\nu_3(T_2)$, which occur between those of $InBr_4^-$ and $SnBr_4$, and the Sn−Se bond length, which occurs between those of $InBr_4^-$ and $CdBr_4^{2-}$. The bending modes, $\nu_2(E)$ and $\nu_4(T_2)$, occur at significantly higher frequencies than in any of the isoelectronic MBX_4 species and may be a consequence of Coulombic repulsion arising from negative charge localization on the chalcogen atoms.

$Sn_4Se_{10}^{4-}$. The fundamental modes of the $Sn_4Se_{10}^{4-}$ anion were assigned under T_d point symmetry and belong to the irreducible representations $\Gamma = 3A_1 + 3E + 3T_1 + 6T_2$. Modes belonging to the A_1, E, and T_2 representations are Raman active, the T_1 modes are inactive, and the T_2 modes are also infrared active. Of the 12 bands expected in the Raman spectrum, the three E modes are expected to have low intensities. A factor-group analysis was performed using the site symmetry of the $Sn_4Se_{10}^{4-}$ anion within the primitive unit cell. Correlation of the free anion symmetry (T_d) with its site symmetry (C_1) to the crystal symmetry (C_i) revealed that a maximum of 12 Raman bands should be observed under C_i crystal symmetry, thus affirming that none of the 12 Raman bands observed in the 50−350-cm^{-1} region arise from factor-group splitting (Table 6).

Raman assignments were made by analogy with those of $Ge_4S_{10}^{4-}$,[33] which was assigned on the basis of polarization measurements and a normal coordinate analysis, and the Sn_4Se_6 fragment of $(CH_3)_4Sn_4Se_6$,[12] which was assigned on the basis of a normal coordinate analysis. Overall, the $Sn_4Se_{10}^{4-}$ anion modes were shifted to lower frequency relative to those of $Ge_4S_{10}^{4-}$ by virtue of the reduced mass effect (Table 6). The most intense band at 178 cm^{-1} was assigned to $\nu_2(A_1)$, the totally symmetric breathing mode of the Sn_4Se_6 cage. The intense band at 274 cm^{-1} was assigned to the totally symmetric stretching mode associated with the terminal Sn−Se bonds and was significantly higher in frequency than $\nu_1(A_1)$ in $SnSe_4^{4-}$ (199 cm^{-1}). An analogous trend has been observed between $Ge_4S_{10}^{4-}$ (457 cm^{-1})[33] and GeS_4^{4-} (386 cm^{-1}).[32] In the cases of $SnSe_4^{4-}$ and GeS_4^{4-}, the negative charge of the anion is localized on the chalcogens, whereas in the adamantanoid $Ge_4S_{10}^{4-}$ and $Sn_4Se_{10}^{4-}$ cages, a significant portion of the negative charge also resides on the bridging chalcogens. Thus, the M−Ch bond lengths in GeS_4^{4-} [2.20(5) Å][49] and $SnSe_4^{4-}$ [2.523(1)−2.516(1) Å][19] are significantly longer than the terminal M−Ch bond lengths in $Ge_4S_{10}^{4-}$ [2.108(11) Å][6] and $Sn_4Se_{10}^{4-}$ [2.416(2)−2.433(2) Å] and are in accord with the observed frequency orders.

Assignments of the A_1 and T_2 fundamentals of the Sn_4Se_6 cage of $Sn_4Se_{10}^{4-}$ are in agreement with the cage modes observed for $(CH_3)_4Sn_4Se_6$, where the $\nu_2(A_1)$ and $\nu_3(A_1)$ counterparts occur at 191(vs) and 80(vs) cm^{-1}, respectively, and the $\nu_{11}(T_2)$ and $\nu_{12}(T_2)$ counterparts occur as site symmetry split bands at 252(s), 248(s) cm^{-1} and 210(m), 208.5(m) cm^{-1}, respectively. With the exception of $\nu_2(A_1)$, these modes occur at lower frequency in the $Sn_4Se_{10}^{4-}$ anion.

The E fundamentals were difficult to assign as they should have low intensities in the Raman spectrum and were not observed for $Ge_4S_{10}^{4-}$ or for the Sn_4Se_6 cage of $(CH_3)_4Sn_4Se_6$ but have been calculated. Consequently, the shoulders at 81 and 290 cm^{-1} were tentatively assigned to the $\nu_4(E)$ and $\nu_5(E)$ modes of $Sn_4Se_{10}^{4-}$. Assignments of the T_2 fundamentals also follow those of $Ge_4S_{10}^{4-}$ except that two components are resolved for the broad weak features assigned to $\nu_{11}(T_2)$ and $\nu_{12}(T_2)$. The splitting is consistent with site symmetry lowering, which leads to removal and partial resolution of the triple degeneracy.

Conclusion

The $Sn_4Se_{10}^{4-}$ anion has been synthesized as its 2,2,2-crypt-K^+ salt. The adamantanoid geometry (T_d point symmetry) of the anion was established in solution by ^{77}Se and ^{119}Sn NMR spectroscopy and in the solid state by X-ray crystallography and Raman spectroscopy. The solution structure of the anion was comfirmed from a detailed analysis of the ^{119}Sn NMR subspectra arising from natural abundance isotopomer distributions, and the $^1J(^{119}Sn-^{77}Se_t)$ and $^1J(^{119}Sn-^{77}Se_b)$ coupling constants were shown to correlate with the Sn−Se_t and Sn−Se_b bond lengths. The terminal Sn−Se stretching frequencies for the $SnSe_4^{4-}$ and $Sn_4Se_{10}^{4-}$ anions are in accord with the relative lengths of the terminal Sn−Se bonds. The vibrational frequencies of $SnSe_4^{4-}$ and SnS_4^{4-} are anomalously high when compared to those of their isoelectronic halide analogues.

Experimental Section

Apparatus and Materials. All compounds used and prepared during the course of this work were air-sensitive. Consequently, all manipulations were carried out under anhydrous and oxygen-free conditions on a glass vacuum line equipped with glass/Teflon grease-free stopcocks (J. Young Scientific Glassware) and in a two-station nitrogen-atmosphere drybox (Vacuum Atmospheres Model DLX). Drybox moisture and oxygen levels were <0.1 ppm.

The oxide layer on large pieces of potassium metal (MCB, >99%), stored under paraffin oil, was cut off and the paraffin oil removed by washing the freshly-cut samples with petroleum ether (Fisher, boiling range 60−80 °C). The metal pieces were rapidly transferred into a dry tube, and the residual ether was removed under vacuum before the clean metal pieces were transferred into the drybox. Prior to use, the residual oxide remaining on the metal surfaces was shaved with a scalpel. Tin shot (Baker Analyzed, 99.9%), selenium powder (Alfa Inorganics, 99.9%), and 2,2,2-crypt (4,7,13,16,21,24-hexaoxa-1,10-diazabicyclo[8.8.8]hexacosane; Merck, 99% or Aldrich, 98%) were used

(49) Philippot, E.; Ribes, M.; Maurin, M. *Rev. Chim. Miner.* **1971**, *8*, 99.

as received and dried in the evacuated port of the drybox for at least 45 min, followed by exposure to the atmosphere of the drybox for at least 2 days prior to use.

All solvents were dried, transferred by vacuum distillation, and stored in round-bottom flasks equipped with glass/Teflon stopcocks. Tetrahydrofuran (Fisher, 99.9%) was stored over sodium wire for several weeks prior to use. Ethylenediamine (Fisher, 99%) was initially dried over CaH_2 (MCB) for several weeks and then vacuum distilled onto, and stored over, fresh CaH_2 for at least an additional week prior to use. Anhydrous ammonia (Canadian Liquid Air or Matheson) was further dried and stored over freshly cut sodium metal at −78 °C for at least 1 week prior to use.

Alloy Fusion and Preparation of the $Sn_4Se_{10}^{4-}$ Solution for NMR Spectroscopy. The alloy, $KSnSe_2$, was prepared as previously described[28] by fusing the elements in the required molar ratios in a thick-walled Pyrex tube (K, 0.9591 g, 24.53 mmol; Sn, 2.7575 g, 23.233 mmol; Se, 3.7318 g, 47.26 mmol). The resulting dark green alloy was ground and its stoichiometry corrected for the recovered tin lump (0.8151 g, 6.867 mmol) to $KSn_{0.67}Se_{1.93}$. The $Sn_4Se_{10}^{4-}$ anion was prepared by extracting the powdered $KSn_{0.67}Se_{1.93}$ alloy in en and liquid NH_3 in the presence of nonstoichiometric amounts of 2,2,2-crypt with respect to K^+. Ethylenediamine solution: $KSn_{0.67}Se_{1.93}$, 0.1710 g, 0.631 mmol; 2,2,2-crypt, 0.0990 g, 0.263 mmol. Liquid NH_3 solution: $KSn_{0.67}Se_{1.93}$, 0.1696 g, 0.626 mmol; 2,2,2-crypt, 0.1000 g, 0.266 mmol.

Multinuclear Magnetic Resonance Spectroscopy. The NMR samples were prepared as described previously.[28] All NMR spectra were recorded on a Bruker AM-500 (11.745 T) pulse spectrometer using a 10-mm probe broad banded over the frequency range 23.3-202.5 MHz and were routinely obtained without locking (field drift < 0.1 Hz h^{-1}). The observing frequencies were 186.504 MHz for ^{119}Sn and 95.384 MHz for ^{77}Se. Free-induction decays were typically accumulated in 32K (^{119}Sn) and 16K (^{77}Se) memories. Spectral width settings of 50 KHz were employed, yielding data point resolutions of 3.052 (^{119}Sn) and 6.104 Hz (^{77}Se) and acquisition times of 0.328 (^{119}Sn) and 0.164 s (^{77}Se), respectively. Relaxation delays were not applied. Typically, 40 000−73 000 (^{119}Sn) and 47 000−90 000 (^{77}Se) transients were accumulated depending on the concentration and the sensitivity of the nuclide under study. Pulse widths corresponding to a bulk magnetization tip angle, θ, of approximately 90° were 15 (^{119}Sn) and 6 μs (^{77}Se). Line broadening parameters used in the exponential multiplication of the free induction decays were 10−30 (^{119}Sn) and 10−20 Hz (^{77}Se). Low-temperature spectra were recorded by using the variable-temperature controller of the spectrometer. Temperatures (accurate to ±1.0 °C and stable to ±0.1 °C) were measured with a copper−constantan thermocouple, which was inserted directly into the sample region of the probe.

The respective nuclei were referenced to neat samples of $(CH_3)_2Se$ and $(CH_3)_4Sn$ at 24 °C. The chemical shift convention used was a positive (negative) sign signifies a chemical shift to high (low) frequency of the reference standard.

The ^{119}Sn subspectra of the $Sn_4Se_{10}^{4-}$ anion were simulated and summed by using the program DSYMPC.[50]

Raman Spectroscopy. Raman spectra were recorded on a Jobin-Yvon Mole S-3000 spectrograph system equipped with a 0.32-m prefilter, adjustable 25-mm entrance slit, and a 1.00-m triple monochromator. Holographic gratings were used for the prefilter (600 groves mm^{-1}, blazed at 500 nm) and monochromator (1800 grooves mm^{-1}, blazed at 550 nm) stages. An Olympus metallurgical microscope (model BHSM-L-2) was used for focusing the excitation laser to a 1-μm spot on the sample. The 514.5-nm line of an Ar ion laser was used for excitation of the samples. Spectra were recorded at ambient temperature on microcrystalline samples sealed in baked-out Pyrex melting point capillaries. Spectra were recorded by signal averaging with a Spectraview-2D CCD detector equipped with a 25-mm chip (1152 × 298 pixels) and at a laser power of 100 mW ($SnSe_4^{4-}$) and 150 mW ($Sn_4Se_{10}^{4-}$) at the sample and slit settings corresponding to a resolution of 1 cm^{-1}. A total of 15 reads having 60- ($SnSe_4^{4-}$) and 90-s ($Sn_4Se_{10}^{4-}$) integration times were used. Spectral line positions are estimated to be accurate to ±1 cm^{-1}.

Crystal Structure Determination of $(2,2,2\text{-crypt-}K^+)_4Sn_4Se_{10}^{4-}$. Crystal Growing. The alloy $KSn_{0.67}Se_{1.93}$ (0.1634 g, 0.603 mmol) was transferred into one arm of a two-arm Pyrex vessel and extracted in en in the presence of a nonstoichiometric amount of 2,2,2-crypt (0.1003 g, 0.267 mmol) with respect to K^+. After 3 weeks, the solution was carefully decanted off the unreacted alloy residue into the second arm of the reaction vessel. An excess of THF (1:2 v:v) was condensed under static vacuum at 0 °C into the first arm of the Pyrex reactor. The reactor was allowed to stand for 4 weeks over which period the THF slowly vapor phase diffused into the yellow-orange en solution, resulting in the formation of a mixture of orange and yellow parallelepiped-shaped crystals just above the supernatant. The mother liquor was decanted back into the first arm of the Pyrex vessel and slowly pumped off under dynamic vacuum. The dry crystalline sample was transferred to a drybox equipped with a stereomicroscope and the reaction vessel cut open. Single crystals of both morphologies were sealed in 0.4-mm Lindemann glass capillaries, which were stored at room temperature prior to mounting on the diffractometer. An analogous liquid NH_3 sample was shown by ^{77}Se and ^{119}Sn NMR spectroscopy to contain mainly the $Sn_2Se_6^{4-}$, $Sn_2Se_7^{4-}$, and $Sn_4Se_{10}^{4-}$ anions as well as a small amount of $SnSe_3^{2-}$ (see **Solution Characterization of $Sn_4Se_{10}^{4-}$ by ^{77}Se and ^{119}Sn NMR Spectroscopy** and ref 15). The Raman spectra of both crystal morphologies were recorded and revealed that the yellow crystal contained the known $Sn_2Se_6^{4-}$ anion[15] and consequently was not further studied by X-ray crystallography. The orange crystal used in this study had the dimensions 0.4 × 0.4 × 0.6 mm^3.

Collection and Reduction of X-ray Data. A crystal of $(2,2,2\text{-crypt-}K^+)_4Sn_4Se_{10}^{4-}$ was centered on a Siemens P4 diffractometer equipped with a rotating anode, using molybdenum radiation monochromatized with a graphite crystal (λ = 0.7107 73 Å). Accurate cell dimensions were determined at room temperature from a least-squares refinement of the setting angles (χ, ϕ and 2θ) obtained from 25 accurately centered reflections (with 22.61° ≤ 2θ ≤ 34.45°) chosen from a variety of points in reciprocal space. Integrated diffraction intensities were collected by using a $\theta-2\theta$ scan technique with scan rates varying from 4.0 to 40° min^{-1} (in 2ω) and a scan range of ±0.34° so that weaker reflections were examined more slowly to minimize counting errors. Data were collected with $-1 \le h \le 15$, $-16 \le k \le 16$, and $-28 \le l \le 28$ and with 5° ≤ 2θ ≤ 45°. During data collection the intensities of three standard reflections were monitored every 97 reflections to check for crystal stability and alignment. A small decay (<8.5%) was observed, which was later corrected by linearly scaling the data between each set of standards. A total of 17 870 reflections were collected, of which 305 were standards. In total, 17 565 reflections were collected and 15 400 unique reflections remained after averaging of equivalent reflections. A total of 10 102 reflections satisfying the condition $I \ge 2\sigma(I)$ were used for structure solution. Corrections were made for Lorentz and polarization effects, and absorption corrections were applied by using the program DIFABS.[51]

Crystal Data. $(2,2,2\text{-crypt-}K^+)_4Sn_4Se_{10}^{4-}$ (f_w = 2926.7 g mol^{-1}) crystallizes in the triclinic system, space group $P\bar{1}$; a = 14.769(2) Å, b = 15.580(1) Å, c = 26.275(4) Å, α = 79.19(1)°, β = 85.65(1)°, γ = 85.870(8)°; V = 5911(1) $Å^3$; D_{calc} = 1.644 g cm^{-3} for Z = 2. Mo Kα radiation [λ = 0.710 73 Å, μ(Mo Kα) = 41.14 cm^{-1}] was used.

Solution and Refinement of the Structure. The XPREP program[52] first confirmed the original cell and showed the lattice to be triclinic primitive (R_{int} = 0.018). A first solution was obtained without absorption corrections. The structure was solved in the space group $P\bar{1}$ (2) by direct methods, which located the general positions of four tin and 10 selenium atoms and indicated the presence of the $Sn_4Se_{10}^{4-}$ anion having an adamantanoid geometry. The full-matrix least-squares refinement of their positions and isotropic thermal parameters gave a conventional R-factor of 0.256. Successive difference Fourier syntheses revealed the general positions of the potassium, nitrogen, oxygen, and

(50) Hägele, G.; Höffken, H.-W.; Mistry, F.; Spiske, R.; Weber, U.; Goudetsidis, S. *DSYMPC*, Release 0.940728E; Institut für Anorganische Chemie und Strukturchemie, Heinrich-Heine-Universität: Düsseldorf, Germany, 1994.

(51) Walker, N.; Struat, D. *Acta Crystallogr.* **1983**, *A39*, 158.

(52) Sheldrick, G. M. *SHELXTL PLUS*, Release 4.21/V; Siemens Analytical X-ray Instruments Inc.: Madison, WI, 1993.

carbon atoms of the four expected 2,2,2-crypt-K^+ cations. A successive full−matrix least−squares refinement of the positions and isotropic thermal parameters of all the atoms, as well as the calculated positions of the hydrogen atoms [d(C−H) = 0.96 Å, $U(H)$ = 0.08 Å^2 was kept fixed], resulted in a significant improvement of the structure (R = 0.114).

The structure was solved a second time by using data that had been corrected for absorption. The Sn, Se, and K atoms were refined with anisotropic thermal parameters. The final refinement was obtained by setting the weight factor to $1/[\sigma^2(F_o^2) + (0.100P)^2 + 0.00P]$ where $P = [\max(F_o^2, 0) + 2F_c^2]/3$ and gave rise to a residual, R_1, of 0.0701 (wR_2 = 0.2024. In the final difference map, the maximum and the minimum electron densities were 1.835 and −0.743 e Å^3.

All calculations were performed on a 486 personal computer by using the SHELXTL PLUS™ package[52] for structure determination, refinement, and molecular graphics.

Acknowledgment. We thank the Natural Sciences and Engineering Research Council of Canada for support in the form of an operating grant (G.J.S.) and for the award of a graduate scholarship (J.C.) and the German Academic Exchange Service (DAAD) for the award of a travel grant (M.W.).

Supporting Information Available: Structure determination parameters for (2,2,2-crypt-K^+)$_4$Sn$_4$Se$_{10}^{4-}$ (Table S1), atomic coordinates and isotropic thermal parameters for the 2,2,2-crypt-K^+ cations (Table S2), distances and angles in the 2,2,2-crypt-K^+ cations (Table S3), anisotropic thermal parameters for (2,2,2-crypt-K^+)$_4$Sn$_4$Se$_{10}^{4-}$ (Table S4), and atomic coordinates for the hydrogen atoms (Table S5) (20 pages). Ordering information is given on any current masthead page.

IC950724P